JOURNAL OF MATERIALS SCIENCE 27 (1992) 5539–5546

A refined statistical approach to thermal fatigue life prediction

F. SUDREAU, C. OLAGNON, G. FANTOZZI
GEMPPM-UA CNRS 341, Bât. 502, INSA, 69621 Villeurbanne Cédex, France
O. LECLERCQ
EMA-EDF Les Renardières, 77250 Moret-sur-Loing, France

Finding new applications for ceramic materials requires a better knowledge of thermal fatigue behaviour. However, result-scattering inherent to thermal fatigue and duration of a thermal fatigue cycle lead to a lack of experimental results. For these reasons, we have developed a new approach that permits the determination of a relevant stress intensity factor exponent n with a minimum testing sample number. From knowledge of the distribution function of artificial cracks, the analytical formula of the failure probability $F(N)$ can be completely determined. Thus, it is possible to calculate n from a correlation of $F(N)$ with experimental results obtained for only one temperature difference. Correlations between theoretical curves $F(N)$ and experimental results, conducted for two temperature differences, lead to the same value of n. This and the good agreement between the experimental points and the theoretical curves validate this new approach.

1. Introduction

Severe thermal shocks on components exhibiting low thermal conductivity and high thermal expansion may induce large thermal stresses. If the stress intensity factor at the most critical flaw reaches its critical value, catastrophic fracture arises causing specimen ruin.

Moreover, even lower thermal shocks may lead to material damage, this phenomenon being defined as thermal fatigue. It is now well recognized that fatigue is the resultant of two specific factors: slow crack growth (static fatigue) and cyclic fatigue.

Slow crack growth, which appears for stress intensity factors lower than material toughness and above a threshold value K_{Iscc}, results from stress corrosion and is therefore strongly environment and temperature dependent.

Cyclic fatigue has been reported in ceramics even for stress intensity factors lower than K_{Iscc}. Although the mechanisms are not fully understood, some possible processes such as debris entrapped within the crack surfaces, which induce indentation-like cracks, or stress intensity increasing during unloading, have been proposed [1, 2].

Under a corrosive environment or at high temperature, the slow crack growth term is often considered as the major fatigue source and has therefore been solely regarded in the case of thermal fatigue.

Thermal fatigue experiments are generally carried out by heating up a specimen which is subsequently quenched. The damage is recorded as a function of the cycle number. The lifetime is defined as the cycle number that makes the most critical crack grow from its initial size up to its critical size that induces a stress intensity factor matching the material toughness.

Clearly, thermal fatigue represents an ultimate material property that limits component applications. However, only a few works have previously been performed because of practical difficulties arising from such studies. Hasselman *et al.* [3, 4] have studied the thermal fatigue behaviour of glass quenched in water. Although their results showed a significant trend between quenching temperature difference and critical cycle number that led to fracture, a tremendous dispersion of the data was noted. A specific testing methodology was set up to overcome this dispersion. While nine starting specimens were concomitantly tested, only five of them were driven to fracture, the cumulative fracture probability of the fifth specimen being considered equal to 0.5. Such a method is time efficient but does not allow the statistical distribution of results to be known.

Glandus and Simonneau [5] investigated the thermal fatigue behaviour of alumina. Their results were analysed with the use of relations, originally established by Singh *et al.* [6], which take into account the temperature dependence of stress corrosion velocity. They pointed out the great dispersion of the results, which has driven them to ignore large critical cycle numbers, since no statistical approach was used.

Kamiya and Kamigaito [7, 8] applied Weibull statistics to their experimental results obtained on glass, Mullite and yttria. The Weibull statistics parameters could not all be determined for the stress state arising from quenching. Moreover, the extrapolation of those parameters from mechanical tests would be erroneous. A specific approach had therefore to be carried out for thermal fatigue results interpretation. This analysis needs the representation of the logarithm of the log-

0022–2461

arithm of the fracture probability versus the logarithm of the critical cycle number, from which straight lines of slopes defined as the Weibull modulus to the stress intensity factor exponent ratio may be plotted, for several temperature differences. The critical cycle numbers, taken for a given probability, may subsequently be represented as a function of temperature difference, which permits the calculation of n. Although interesting because of the statistical approach, this methodology has several drawbacks. Owing to the choice of the scale (lnln–ln), the precision is relatively poor. Furthermore, two steps are required to obtain the stress intensity factor exponent value, which can be known with sufficient precision only under the condition of testing a significant number of temperature differences.

This brief survey describing the main approaches presented in the literature emphasizes the experimental difficulties arising during thermal fatigue experiments:

(i) Thermal fatigue cycles are generally long, especially compared with mechanical cycling that can easily be achieved at frequencies equal to 10 Hz. Thermal fatigue characterization is therefore very time consuming.
(ii) The intrinsic flaw size distribution is enhanced by the slow crack growth propagation laws (power-like laws) leading to extremely dispersed results.

Moreover, the two above, apparently separate, problems synergetically lead to a further obstacle such that problem (ii) would require large numbers of experiments that are difficult to achieve owing to problem (i).

Therefore, a precise statistical methodology with fully defined expressions has to be applied to improve thermal fatigue characterization. To achieve this target, the present work proposes a new approach, i.e. creating artificial flaws in the samples, which brings several advantages:

(i) The initial flaw size distribution may be narrowed.
(ii) The initial flaw size distribution function may be precisely known.
(iii) The critical defects being at the centre of the specimens, any edge effects may be avoided, leading to better known stress fields.

The measured initial crack size distribution (explicitly known) is subsequently combined with the slow crack growth law in order to define the cumulative fracture probability as a function of thermal cycle number.

2. Theory

The objective of this part is to determine the analytical expression, for a given temperature difference, of the cumulative probability of fracture as a function of critical cycle number. First, the probability density of initial crack size is evaluated and related to the probability density of critical cycle number.

2.1. Artificial flaws

The starting cracks were made by Vickers indentation under the condition of having half penny shape cracks.

The prerequisite of the present analysis being that the flaw distribution is definitely known, a Gaussian distribution law has been chosen as the starting hypothesis. This hypothesis will need experimental confirmation (see below). The probability density as a function of flaw size is therefore given by:

$$f_a(a_i) = \frac{1}{s_d(2\pi)^{1/2}} \exp\left[-\frac{1}{2}\left(\frac{a_i - \langle a \rangle}{s_d} \right)^2 \right] \quad (1)$$

where a_i is the initial flaw size, s_d the standard deviation and $\langle a \rangle$ the average flaw size for given indentation load and material.

The probability densities of critical cycle number and crack size are defined as

$$f(N) = \frac{P(N < N_0 < N + dN)}{dN} \quad (2)$$

and

$$f_a(a_i) = \frac{P(a_i < a_{i0} < a_i + da_i)}{da_i} \quad (2')$$

where $P(N < N_0 < N + dN)$ and $P(a_i < a_{i0} < a_i + da_i)$ represent the probabilities that the critical thermal cycle number and the initial crack size are in the range N to $N + dN$ and a_i to $a_i + da_i$, respectively.

The probability densities of initial crack size and critical cycle number are therefore related as

$$f(N) = -f_a(a_i)\frac{da_i}{dN} \quad (3)$$

Note that the negative sign is due to the fact that the probability for a critical cycle number to be lower than a given value is equal to the probability for an initial crack size to be higher than a related given value.

Equation 3 can be explicitly given as a function of the critical cycle number using Equation 1 after having determined the function $a_i(N)$.

2.2. Thermal fatigue

The slow crack growth velocity is assumed to be equal to that conventionally reported under isothermal conditions [6]

$$\frac{da}{dt} = AK_I^n \exp\left(-\frac{Q}{RT} \right) \quad (4)$$

where a is the crack size, K_I the mode I stress intensity factor, A a material constant, n the stress intensity factor exponent, Q the thermal activation energy, T the temperature and R the gas constant.

The stress intensity factor is related to the crack size and to the applied stress according to

$$K_I = Y\sigma_T a^{1/2} \quad (5)$$

where Y is a geometrical factor and σ_T is the thermal stress induced by quenching. Analysis of quenching stresses shows that the sample surface is submitted to a biaxial tensile stress. Moreover, the tensile stress rapidly decreases along the sample depth and the core

is under compression. Precise calculations as well as experiments have shown that for water quenching (high surface exchange coefficient) the tensile stress zone depth is very small, leading to nearly surface crack propagation. Therefore, only the maximum tensile stress (i.e., the surface stress), which is an explicit function of the time, has been considered for the calculation.

Badaliance *et al.* [9] have shown that the surface stress calculated from heat transfer equations could be expressed as

$$\sigma_T(t) = \Delta T f_B(t) \tag{6}$$

where ΔT is the temperature difference between hot temperature and quenching medium temperature and $f_B(t)$ is a function of the time given for a material, a sample shape and a quenching medium. Substituting Equations 5 and 6 into Equation 4 and integrating over the quenching time μ, the following relation is obtained [7]

$$a_i = N^{2/(2-n)}\left(\frac{n-2}{2}\right)^{2/(2-n)}\left(AY^n\exp\left(-\frac{Q}{RT}\right)\right. \times \left.\int_0^{\mu} f_B^n(t)\,dt\right)^{2/(2-n)} \Delta T^{2n/(2-n)} \tag{7}$$

where N is the critical cycle number. It is to be noted that Equation 7 has been obtained under the following assumption on the critical crack size a_f (i.e. the crack size after N thermal cycles)

$$a_f^{(2-n)/2} \ll a_i^{(2-n)/2} \tag{8}$$

which implies that the temperature difference ΔT is much smaller than the critical temperature difference leading to thermal shock (fracture during the first cycle) or that $n \gg 1$. While the former assumption is almost never verified in laboratory conditions, the latter is generally satisfied. This will be confirmed in a following part. If those hypotheses cannot be satisfied, the critical flaw size must be included in Equation 7.

The probability density as a function of thermal cycle number is subsequently obtained by substituting the derivative of Equation 7 with respect to N as well as Equation 1 into Equation 3.

$$f(N) = \frac{1}{s_d(2\pi)^{1/2}}\exp\left[-\frac{\left(\left(N\left(\frac{n-2}{2}\right)G(T,n)\Delta T^n\right)^{2/(2-n)} - \langle a\rangle\right)^2}{2s_d^2}\right]\left(\left(\frac{n-2}{2}\right)^n N^n G(T,n)^2\Delta T^{2n}\right)^{1/(2-n)} \tag{9}$$

with

$$G(T,n) = AY^n\exp\left(-\frac{Q}{RT}\right)\int_0^{\mu} f_B^n(t)\,dt \tag{9'}$$

Given that, the failure probability can be expressed as

$$F(N_r) = \frac{\left(\left(\frac{n-2}{2}\right)^n G(T,n)^2\cdot\Delta T^{2n}\right)^{1/(2-n)}}{s_d(2\pi)^{1/2}}\int_0^{N_r}\exp\left[-\frac{\left(\left(N\left(\frac{n-2}{2}\right)G(T,n)\cdot\Delta T^n\right)^{2/(2-n)} - \langle a\rangle\right)^2}{2s_d^2}\right]N^{n/(2-n)}\,dN \tag{10}$$

The failure probability is therefore explicitly expressed as a function of the variable N, the parameters ΔT, s_d, $\langle a\rangle$ and n, and the $G(T, n)$ function that needs to be clearly expressed.

2.3. Determination of $G(T, n)$

Equation 9′ can be written as

$$\ln(G(T,n)) = \ln(A) - \frac{Q}{RT} + n\ln(Y) + \ln(I(n)) \tag{11}$$

with

$$I(n) = \int_0^{\mu} f_B^n(t)\,dt \tag{11'}$$

$f_B(t)$ has been expressed by Badaliance *et al.* [9] for a long cylindrical rod subjected to radial heat flow as the result of an instantaneous decrease in ambient temperature, with conductive heat transfer in the solid and convective heat transfer in the surrounding medium. It is to be noted that an analytical expression is found if the thermal conductivity and the Young's modulus are constant over the considered temperature range. Otherwise, finite elemental calculation must be performed. Assuming that the transient thermal stress ($\sigma T(t)$) is similar for a rectangular section bar, $f_B(t)$ can be written as

$$f_B(t) = \left(\frac{E\alpha}{1-\nu}\right)2\left[\sum_{i=1}^{\infty} v_i\exp\left(-\frac{\eta_i^2\kappa}{e^2}t\right)\right] \tag{12}$$

with

$$v_i = \frac{J_1(\eta_i)}{(\beta^2+\eta_i^2)J_0^2(\eta_i)}[2J_1(\eta_i) - \eta_i J_0(\eta_i)] \tag{12'}$$

where E is the elastic modulus, α the linear thermal expansion coefficient, ν the Poisson ratio, β the Biot modulus, e the half thickness of the bar, κ the thermal diffusivity, J_0 and J_1 the Bessel functions of the zero and first order, and η_n the root of $\beta J_0(\eta_n) - \eta_n J_1(\eta_n) = 0$.

$G(T, n)$ is so far fully defined as an analytical function of n and T. The $G(T, n)$ expression can be simplified following approximations and calculations detailed in Appendix 1. Thus, $G(T, n)$ can be expressed

as:

$$\ln(G(T, n)) = \ln(A) - Q/(RT) + n\ln(2E\alpha v_1 Y/(1 - \nu)) + D \quad (13)$$

where D is a constant.

Finally, for a given artificial flaw size distribution, the fracture probability $F(N)$ only depends on n, T and ΔT. Therefore, the experimental value of n may be found from the best fitting of experimental points, obtained at a given ΔT, by the theoretical curve $F(N)$.

3. Experimental procedure

The following experiments have been carried out to examine the validity of the above approach.

3.1. Specimens

The specimens were mullite bars of rectangular section with dimensions $40 \times 4 \times 2$ mm^3. Their chemical composition and physical properties are given in Table I. The edges of the bars had been polished with 1200 grit silicon carbide paper. A Vickers indentation was made on a face centre with an applied load of 20 N for 15 s. The specimens were further heated and held at 1000 °C for 1 h in order to release residual stresses induced by indentation.

3.2. Determination of the crack size distribution function

To find the crack size distribution function, 19 Vickers indentations were made on a Mullite bar. The crack lengths were measured on the specimen surface by optical microscopy. For each length, the cumulative probability $F_a(a_i)$ was taken as the fraction given by dividing the number of lengths $\leqslant a_i$ by the total number of measured lengths, 19.

Having calculated the experimental values $F_a(a_i)$, the average $\langle a \rangle$ and the standard deviation s_d allowing the best fitting between the experimental points and a normal law were determined. The best fitting was obtained taking $\langle a \rangle = 183$ μm and $s_d = 14$ μm (Fig. 1). It should be noted that a good agreement was achieved, which validates the assumption that the artificial crack size distribution function can be well described by a Gaussian law.

3.3. Apparatus and experimental procedure

The apparatus consists of a hot zone in an electric resistance furnace, a cold zone in a 20 °C regulated water tank and a transfer system. The time for the transfer from the hot zone to the water was about 1 s and that from the water to the hot zone about 25 s. The sample was held in the hot zone for 10 min and in the cold zone for 40 s.

The temperature difference ΔT in the formulae has been taken as the difference between the temperature of the hot zone, T, and that of the water. The failure of a specimen was determined by the occurrence of a visible crack on the sample surface. Detection of a visible crack on specimens was recorded, by use of dye penetrant, at a given thermal cycle number. The failure probability F has been taken as the ratio of the number of fractured specimens after a given thermal cycle number to the total number of tested specimens.

3.4. Numerical expression of $G(T, n)$

Since the A and Y constants in Equation 9′ cannot be known with high accuracy, the numerical function of $G(T, n)$ has been experimentally determined. Seven samples were tested with a hot temperature equal to 285 °C, i.e. $\Delta T = 265$ °C (see Table II). Knowing s_d and $\langle a \rangle$, the theoretical distribution function $F(N)$ can be calculated for given n and $G(285, n)$ values. Thus, the values of $G(285, n)$ that give the best fitting between experimental points and the theoretical distribution function have been calculated for ten values of n in the range 20–110. The accuracy of the fitting has been quantified by the value $S(G)$, defined as the sum of the distances between the experimental points

TABLE I Chemical composition and physical properties of the specimens of Mullite

Characteristics		Value
Chemical[a]	Chemical composition (wt %):	
	Al_2O_3	76.4
	SiO_2	22.8
	$Na_2O + K_2O$	< 0.5
	Other impurities	< 0.3
Physical[a]	Open porosity (vol %)	0
	Apparent bulk density (kg m$^{-3} \times 10^3$)	> 3.07
	Theoretical density (kg m$^{-3} \times 10^3$)	3.15
Thermal[a]	Coefficient of linear expansion (K$^{-1} \times 10^{-6}$) (20/500 °C)	4.8
	Thermal conductivity (at 20 °C) (Wm^{-1} K^{-1})	4.4
	Specific heat (at 100 °C) (J kg^{-1} K^{-1})	900
Mechanical	Mechanical strength, 4-point bending (at 20 °C) (MPa)[b]	234
	Young's modulus (at 20 °C) (GPa)[b]	190
	Poisson's modulus (at 20 °C)[a]	0.28
	K_{Ic} Toughness (at 20 °C) (MPa M$^{1/2}$)[b]	2.6

[a] Data given by the manufacturer (Céramiques et Composites, Bazet, France).
[b] Data measured by the authors.

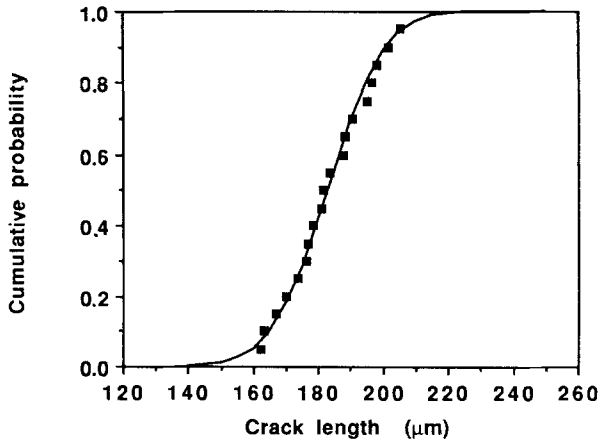

Figure 1 Measured indentation crack size and theoretical normal law ($\langle a \rangle = 183$ μm and $s_d = 14$ μm). ■, Experimental points; ——, theoretical normal law.

TABLE II Experimental critical thermal cycle numbers four different values of ΔT

Sample no.	ΔT (°C)			
	270	265	260	255
N_1	1	4	34	20
N_2	19	10	58	318
N_3	32	10	102	546[a]
N_4		38	710	1564[a]
N_5		94	738	1776[a]
N_6		290		
N_7		318[a]		

[a] Samples with no visible crack after the reported thermal cycle number.

and the theoretical curve. Plotting $\ln(G(285, n))$ versus n has allowed the calculation of the numerical function $G(285, n)$ (Fig. 2) which was found to be: $G(285, n) = \exp(-1.28n - 15)$.

4. Results

Only four parameters are so far required to calculate the distribution function $F(N)$. Three of those parameters have been experimentally fixed, $s_d = 14$ μm, $\langle a \rangle = 183$ μm and $\Delta T = 265$ °C. Thus, n was the sole unknown parameter in Equation 10. It has been obtained from the best fitting between the experimental points and the theoretical distribution function curve, $F(N)$. The sum $S(n)$ taken as the sum of the distances between the experimental points and the theoretical distribution function curve has again been chosen as the fitting accuracy criterion.

Fig. 3 represents S as a function of n and shows a minimum at $n = 55$. The stress intensity factor exponent of this Mullite, submitted to water quenching, is therefore equal to 55. Note that this result is in the wide range reported in the literature for oxide materials [5, 7]. Moreover, the assumption under which Equation 7 was obtained, i.e. $n \gg 1$, was justified.

Fig. 4 shows the distribution function versus the thermal cycle number. The good agreement between experiments and the theoretical curve $F(N)$ validates Equation 10.

To confirm the n value found for $\Delta T = 265$ °C, other tests have been carried out for $\Delta T = 260$ °C (see Table II). Considering the small temperature range investigated, i.e. 275–290 °C, the term $-Q/RT$ of Equation 13 has been assumed to be constant. This assumption has been verified for $T = 280$ °C (see Fig. 2). Thus, the same $G(T, n)$ numerical function has been taken for the whole temperature range tested.

The same analysis as that applied for $\Delta T = 265$ °C has led to $n = 53$ for $\Delta T = 260$ °C (Fig. 5). From this

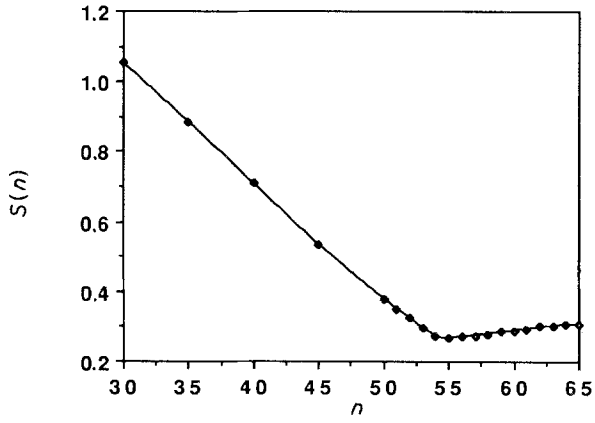

Figure 3 Sum of the distances between the experimental points and the theoretical curve $F(N)$ as a function of the stress intensity factor exponent ($\Delta T = 265$ °C).

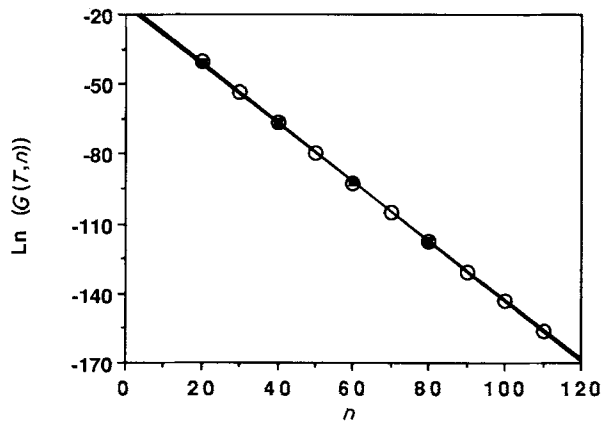

Figure 2 $G(T, n)$ functions experimentally determined at ○, $T = 285$ °C and ■, $T = 280$ °C.

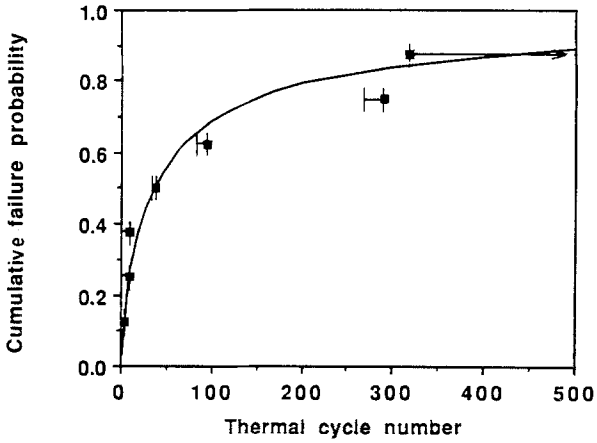

Figure 4 Cumulative failure probability as a function of thermal cycle number ($\Delta T = 265$ °C; $\langle a \rangle = 183$ μm and $s_d = 14$ μm). ■, Experimental points; ——, theoretical curve.

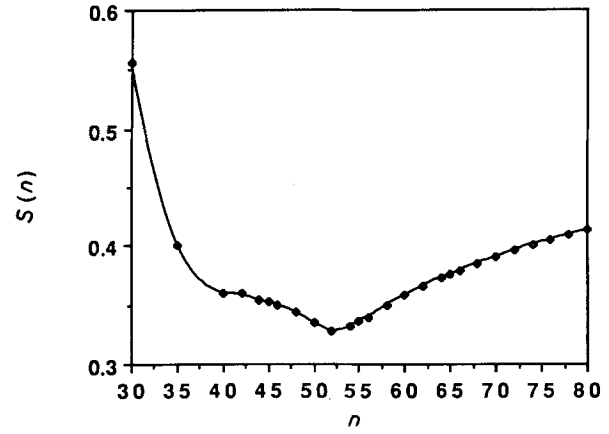

Figure 5 Sum of the distances between the experimental points and the theoretical curve $F(N)$ as a function of the stress intensity factor exponent ($\Delta T = 260\,°C$).

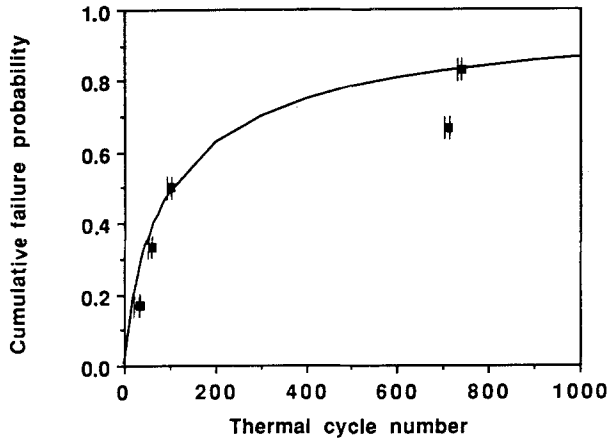

Figure 6 Cumulative failure probability as a function of thermal cycle number ($\Delta T = 260\,°C$; $\langle a \rangle = 183\,\mu m$ and $s_d = 14\,\mu m$). ■, Experimental points; ——, theoretical curve.

value, the theoretical distribution function has been calculated (Fig. 6).

Some tests have also been carried out with $\Delta T = 255\,°C$ and $\Delta T = 270\,°C$. Although it has not been possible to determine a relevant value of n with the few samples tested (see Table II), the theoretical distribution functions calculated taking the previous value of $n (n = 53)$ have been plotted for $\Delta T = 270\,°C$ and $\Delta T = 255\,°C$ in Fig. 7.

5. Discussion

In order to link this approach with those generally used, the authors have defined some representative values of critical cycle numbers which can be plotted as a function of ΔT.

From Equation 7, one can write [7] for samples having the same initial crack size

$$\ln(N) = -n\ln(\Delta T) + Z \qquad (14)$$

where Z is a constant. Thus, plotting $\ln(N)$ versus $\ln(\Delta T)$ allows the calculation of n. Although having a constant initial crack size is experimentally impossible, the knowledge of initial crack size distribution function and failure probability function allows values

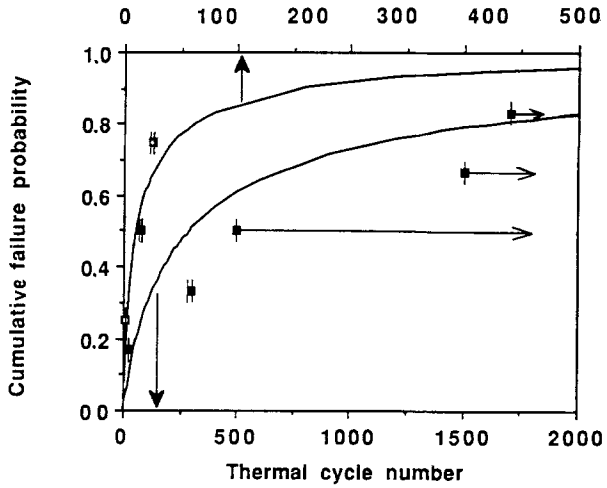

Figure 7 Cumulative failure probability as a function of thermal cycle number (□, $\Delta T = 270\,°C$ and ■, $\Delta T = 255\,°C$; $\langle a \rangle = 183\,\mu m$ and $s_d = 14\,\mu m$).

of N which correspond to a given initial crack size to be calculated. For instance, one can calculate the critical cycle numbers which agree with an initial crack size $a_{i,x}$. From this initial crack size, the cumulated probability $F_a(a_{i,x}) = P(a_i \leqslant a_{i,x}) = x$ and the corresponding thermal cycle number N_x defined by $F(N_x) = P(N \leqslant N_x) = 1 - x$ could be calculated. In the present case, the critical cycle number representative values which agree with an initial crack size $a_{i,0.5} = \langle a \rangle = 183\,\mu m$, have been calculated. Those values of $N_{0.5}$ defined by $F(N_{0.5}) = 0.5$ are reported in Table III.

Another example of critical cycle number representative values is the group of critical cycle numbers defined by $df(N_M)/dN = 0$. For those cycle numbers, the failure probability density function is maximum and the corresponding initial crack size is: $a_{i,M} = (\langle a \rangle + (\langle a \rangle^2 + 2n s_d^2)^{1/2})/2$ (see Appendix 2). Experimental conditions described in this paper lead to $a_{i,M} = 208\,\mu m$ and the calculated values of N_M are reported in Table III. The N_M values are much smaller than the critical cycle numbers found experimentally due to the fact that they agree with a large initial crack size ($a_{i,M} = \langle a \rangle + 1.8\,s_d$).

Both examples of critical thermal cycle numbers are plotted as a function of temperature difference ΔT in Fig. 8. The two least square straight lines run parallel with a slope equal to -54. Fig. 8 clearly shows that when the failure probability and the crack size distribution function are well defined, the thermal fatigue behaviour can be described by several kinds of thermal cycle number representative values calculated from a constant initial crack size.

TABLE III Representative values of thermal cycle numbers

ΔT (°C)	n	$N_{0.5}$	N_M
270	–[a]	14	0.5
265	55	36	1.1
260	53	104	4
255	–[a]	288	11

[a] Value not known.

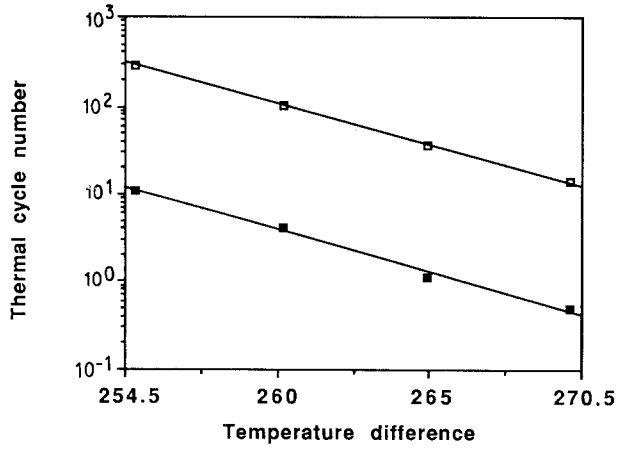

Figure 8 Representative values of thermal cycle numbers as a function of ΔT. The slope of the straight lines is equal to -54. □, N such as $F(N) = 0.5$; ■, N such as $df(N)/dN = 0$.

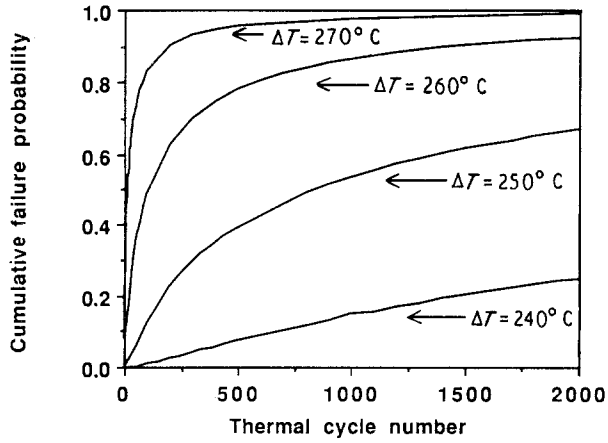

Figure 9 Theoretical cumulative failure probability curves as a function of thermal cycle number for four values of ΔT.

It should also be noted that the thermal activation energy Q could be determined from the approach presented in this paper. Indeed, Equation 13 can be rewritten as:

$$\ln(G(T, n)) = cn + d(T) \quad (15)$$

where c and $d(T)$ are experimentally known values for a given temperature. Thus, determining the numerical expressions $G(T, n)$ at two temperatures T_1 and T_2 allows the calculation

$$Q = (R(d(T_1) - d(T_2)))\left(\frac{1}{T_2} - \frac{1}{T_1}\right)^{-1} \quad (16)$$

However, under usual laboratory conditions, T_1 and T_2 are too close for a relevant determination of the thermal activation energy. Thus, if this value has to be known with high accuracy, mechanical tests seem to be unavoidable.

Finally, Fig. 9 shows theoretical failure probability curves as a function of thermal cycle number, for several values of ΔT. Those curves illustrate the rapid increase of the result scattering even for experiments carried out at ΔT close to the critical temperature difference with pre-indented specimens. This confirms the practical difficulties in obtaining the thermal fatigue parameters n and Q under industrial environments (i.e. $\Delta T \ll \Delta T_c$). Finding relations between mechanical fatigue behaviour of ceramic materials could be a way to overcome those difficulties.

6. Conclusion

A refined statistical approach has been developed to determine the stress intensity factor exponent n with a minimum testing sample number. This approach is based on the knowledge of the artificial crack size distribution function and allows the whole determination of the failure probability analytical expression. From this expression the n value can be calculated with experiments carried out under only one temperature difference.

This approach has been validated with experiments on Mullite with two temperature differences. Both n values found have been shown to be very close, and a good agreement between experimental points and theoretical curves has been obtained.

This new approach allows the study of the thermal fatigue behaviour of ceramic materials with a reasonable experimental time and high accuracy. Understanding of the material damage phenomena arising during thermal fatigue and in turn the life prediction of the ceramic components may therefore be improved.

Appendix 1

Substituting Equation 12 in Equation 11′, $I(n)$ can be written

$$I(n) = \left(\frac{E\alpha}{1-\nu}\right)^n 2^n \cdot \int_0^{\mu}\left[\sum_{i=1}^{\infty} v_i \cdot \exp\left(-\frac{\eta_i^2 \kappa}{e^2} t\right)\right]^n dt \quad (A11)$$

Since the terms of the sum rapidly converge to zero, only the first five terms are needed to calculate values of the $f_B(t)$ function with high accuracy. Thus, using the general binomial formula

$$(x_1 + x_2 + \cdots + x_p)^n = \sum \frac{n!}{n_1! n_2! \ldots . n_p!} x_1^{n_1} x_2^{n_2} \ldots . x_p^{n_p} \quad (A12)$$

where the sum Σ is taken for all integers $n_1, n_2, \ldots, n_p$ such that $n_1 + n_2 + \cdots + n_p = n$, $I(n)$ can be rewritten as

$$I(n) = \left(\frac{E\alpha}{1-\nu}\right)^n 2^n \int_0^{\mu}\left[\sum \frac{n!}{n_1! n_2! \ldots n_5!} \times \prod_{i=1}^{5} v_i^{n_i} \cdot \exp\left(-\frac{\eta_i^2 \kappa n_i}{e^2} t\right)\right] dt \quad (A13)$$

This expression can be integrated, giving

$$I(n) = \left(\frac{E\alpha}{1-\nu}\right)^n 2^n \left[\sum \frac{n!}{n_1! n_2! \ldots n_5!} \cdot \prod_{i=1}^{5} (v_i^{n_i}) \cdot \left(\frac{\exp(-\kappa e^{-2}(\eta_1^2 n_1 + \eta_2^2 n_2 + \cdots + \eta_5^2 n_5)\mu) - 1}{-\kappa e^{-2}(\eta_1^2 n_1 + \eta_2^2 n_2 + \cdots + \eta_5^2 n_5)}\right)\right] \quad (A14)$$

If it is assumed that the term such as: $n_1 = n$ and $n_2 = n_3 = n_4 = n_5 = 0$ is much greater than the others, and that

$$\exp\left(-\frac{\kappa}{e^2}(\eta_1^2 n_1 + \eta_2^2 n_2 + \cdots + \eta_5^2 n_5)\mu \right) \ll 1$$

I(n) can be simply expressed by

$$\mathrm{I}(n) = \left(\frac{E\alpha}{1-\nu}\right)^n 2^n \frac{v_1^n}{\kappa e^{-2}\eta_1^2 n} \qquad \text{(A15)}$$

therefore

$$\ln(\mathrm{I}(n)) = n\ln\left(\frac{2E\alpha v_1}{1-\nu}\right) - \ln(n) - \ln\left(\frac{\kappa}{e^2}\eta_1^2\right) \qquad \text{(A16)}$$

In order to verify both assumptions mentioned above, integral I(n) has been numerically calculated from Equation (A11) and from Equation A16. It can be seen in Fig. A1 that for n increasing from 20 to 110, the two equations lead to almost the same I(n) values. Moreover, in Equation A16, for n values in the range 20–110, ln(n) can be considered as constant compared with the increase of the $n\ln(2E\alpha v_1/(1-\nu))$ term. Thus, I(n) can be expressed as

$$\ln(\mathrm{I}(n)) = n\ln(2E\alpha v_1/(1-\nu)) + D \qquad \text{(A17)}$$

with

$$D = -\ln(n) - \ln(\kappa\eta_1^2/e^2) \qquad \text{(A17')}$$

Substituting Equation A17 into Equation 11 gives Equation 13, namely

$$\ln(G(T,n)) = \ln(A) - Q/(RT) + n\ln(2E\alpha v_1 Y/(1-\nu)) + D$$

Appendix 2

The critical cycle number N_M is defined by

$$\frac{df(N_M)}{dN} = 0 \qquad \text{(A21)}$$

where, from Equation 3

$$f(N) = -f_a(a_i)\frac{da_i}{dN}$$

One can therefore write

$$\frac{df(N)}{dN} = -\left[\frac{df_a(a_i)}{da_i}\left(\frac{da_i}{dN}\right)^2 + f_a(a_i)\frac{d^2a_i}{dN^2}\right] \qquad \text{(A22)}$$

Moreover, with the definition of the normal law (Equation 1)

$$f_a(a_i) = \frac{1}{s_d(2\pi)^{1/2}}\exp\left[-\frac{1}{2}\left(\frac{a_i - \langle a\rangle}{s_d}\right)^2\right]$$

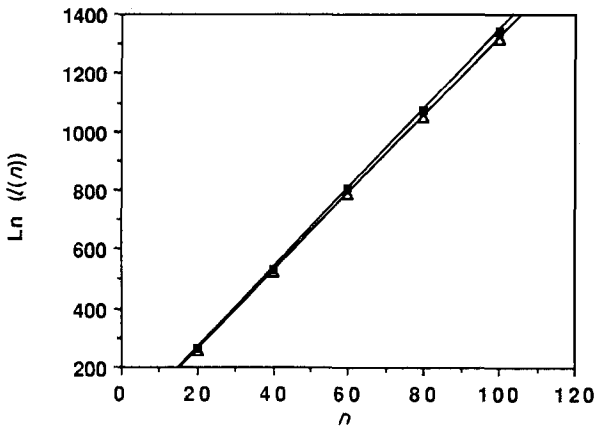

Figure A1 Values of integral I as a function of the stress intensity factor exponent calculated from the original and simplified equations ($E = 207$ GPa; $\alpha = 4.8 \times 10^{-6}\ \mathrm{K}^{-1}$; $\nu = 0.28$; $v_1 = 0.264$; $\kappa = 1.3 \times 10^{-6}\ \mathrm{m^2\,s}$; $R = 10^{-3}$ m; $\eta_1 = 1.99$). △, Calculated from Equation A11; ■, calculated from Equation A16.

and the relation (Equation 7)

$$a_i(N) = N^{2/(2-n)} \cdot \left(\frac{n-2}{2}\right)^{2/(2-n)} \times G(T,n)^{2/(2-n)} \Delta T^{(2n)/(2-n)}$$

$df(N)/dN$ can be written as

$$\frac{df(N)}{dN} = -f_a(a_i)\frac{2a_i}{N^2(2-n)^2}\left[\frac{2(a_i - \langle a\rangle)a_i}{-s_d^2} + n\right] \qquad \text{(A23)}$$

Since a_i and $f_a(a_i)$ do not equal zero, the condition $df(N_M)/dN = 0$ agrees with:

$$a_{i,M} = \frac{\langle a\rangle + (\langle a\rangle^2 + 2ns_d^2)^{1/2}}{2} \qquad \text{(A24)}$$

which is the single positive solution.

References

1. S. HORIBE, *J. Eur. Ceram. Soc.* **6** (1990) 89.
2. M. J. REECE, F. GUIU and M. F. R. SAMMUR, *J. Am. Ceram. Soc.* **72**[2] (1989) 348.
3. D. P. H. HASSELMAN, R. BADALIANCE and E. P. CHEN, in "Thermal Fatigue of Materials and Components" (Proceedings of the Symposium, New Orleans, 1975), (American Society for Testing and Materials, Philadelphia, 1976) p. 55.
4. D. P. H. HASSELMAN, E. P. CHEN, C. L. AMMANN, J. E. DOHERTY and C. G. NESSLER, *J. Amer. Ceram. Soc.* **58** [11–12] (1975) 513.
5. A. M. SIMONNEAU, "Resistance aux chocs thermiques et à la fatigue thermique de céramiques thermomécaniques. Influence des conditions expérimentales." (Thèse de doctorat, université de Limoges, 1989) p. 134.
6. J. P. SINGH, K. NIIHARA and D. P. H. HASSELMAN, in "Thermo-mechanical and Thermal Behavior of High Temperature Structural Materials", (Interim Report to Office of Naval Research, 1981) Ch. 4.
7. N. KAMIYA and O. KAMIGAITO, *J. Mater. Sci.* **14** (1979) 573.
8. *Idem., ibid.* **24** (1989) 246.
9. R. BADALIANCE, D. A. KROHN and D. P. H. HASSELMAN, *J. Amer. Ceram. Soc.* **57**[10] (1974) 432.

Received 26 June
and accepted 27 November 1991